Analytical model of the nonlinear dynamics of cantilever tip-sample surface interactions for various acoustic-atomic force microscopies

John H. Cantrell

NASA Langley Research Center, Mail Stop 231, Hampton, Virginia 23681

and

Sean A. Cantrell

Department of Physics, University of Virginia, Charlottesville, Virginia 22904

(Received

A comprehensive analytical model of the interaction of the cantilever tip of the atomic force microscope (AFM) with the sample surface is developed that accounts for the nonlinearity of the tip-surface interaction force. The interaction is modeled as a nonlinear spring coupled at opposite ends to linear springs representing cantilever and sample surface oscillators. The model leads to a pair of coupled nonlinear differential equations that are solved analytically using a standard iteration procedure. Solutions are obtained for the phase and amplitude signals generated by various acoustic-atomic force microscope (A-AFM) techniques including force modulation microscopy, atomic force acoustic microscopy, ultrasonic force microscopy, heterodyne force microscopy, resonant difference-frequency atomic force ultrasonic microscopy (RDF-AFUM), and the commonly used intermittent contact mode (TappingMode) generally available on AFMs. The solutions are used to obtain a quantitative measure of image contrast resulting from variations in the Young modulus of the sample for the amplitude and phase images generated by the A-AFM techniques. Application of the model to RDF-AFUM and intermittent soft contact phase images of LaRC-cp2 polyimide polymer is discussed. The model predicts variations in the Young modulus of the material of 24 percent from the RDF-AFUM image and 18 percent from the intermittent soft contact image. Both predictions are in good agreement with the literature value of 21 percent obtained from independent, macroscopic measurements of sheet polymer material.

PACS numbers: 68.37.Tj, 81.07.-b, 82.35.Np, 68.37.-d

I. INTRODUCTION

The atomic force microscope[1] (AFM) has become an important nanoscale characterization tool for the development of novel materials and devices. Dynamic implementations of the AFM (we shall call acoustic-atomic force microscopies or A-AFM)) such as intermittent contact mode (TappingMode), force modulation microscopy[2] (FMM), atomic force acoustic microscopy[3-4] (AFAM), ultrasonic force microscopy[5-6] (UFM), heterodyne force microscopy[7-8] (HFM), resonant difference-frequency atomic force ultrasonic microscopy[9] (RDF-AFUM) and variations of these techniques[10-14] utilize the interaction force between the cantilever tip and the sample surface to extract information about sample material properties. Such properties include sample elastic moduli, adhesion, surface viscoelasticity, embedded particle distributions, and topography. The cantilever tip-sample surface interaction force is generally nonlinear[5], although in some operational modes the interaction force can be taken to a good approximation to be linear. A comprehensive treatment of the interaction force, however, is lacking because of the difficulty in accounting for the nonlinear terms. We consider here a detailed analytical treatment of the cantilever tip-sample surface interaction force that includes the lowest-order terms in the nonlinearity. Such terms are sufficient to account for all operational characteristics and material properties obtained from the various acoustic-atomic force microscopies cited above.

We begin in Section II by developing a realistic mathematical model of the interaction between the cantilever tip and the sample surface that involves a coupling via the nonlinear interaction force of separate dynamical equations for the cantilever and the sample surface. A general solution is found that contains static terms (including static

terms generated by the nonlinearity), linear oscillatory terms, and nonlinear oscillatory terms. Individual or various combinations of these terms are found to apply as appropriate to a description of a particular acoustic-atomic force microscopy. The complexity of the general solution begs consideration of ways to simplify the mathematical expression by estimating the relative magnitudes of the material and dynamical parameters embedded in the equation. Such estimates are considered in Section III. Application of the solution to each of the above-cited acoustic-atomic force microscopies is given in Section IV using simplifications resulting from the estimate of parameter values obtained in Section III. Section V provides an analytical analysis of image contrast for each of the A-AFM techniques addressed in the model. Application of the model to RDF-AFUM and intermittent soft contact phase images of LaRC-cp2 polyimide polymer is discussed in Section VI.

II. ANALYTICAL MODEL OF NONLINEAR CANTILEVER DYNAMICS

A. General dynamical equations

The cantilever of the AFM is able to vibrate in a number of different modes in free space corresponding to various displacement types (flexural, longitudinal, shear, etc.), resonant frequencies, and effective stiffness constants. Each cantilever mode n of a given displacement type may be represented by an effective mass m_c attached to a spring of stiffness constant k_{cn} and resonant frequency $\omega_{cn} = \sqrt{k_{cn} / m_c}$. Since each mode is subject to the same driving forces, we may express the cantilever time-dependent displacement η_c in its most general form as the sum over all modes and write

$$\eta_c(t) = \sum_n \eta_{cn}(t) \qquad (1)$$

where η_{cn} is the cantilever displacement corresponding to mode n and t is time. During contact of the cantilever with the sample surface, vibrations of the cantilever give rise to oscillations of the sample surface via the cantilever tip-sample surface interaction forces. Likewise, an oscillating sample surface resulting, for example, from an incident ultrasonic wave generated at the opposite surface of the sample will also give rise to oscillations of the cantilever via the same interaction forces. The vibrating sample surface may be represented by an effective mass m_s attached to a spring of stiffness constant k_s.

For definiteness we consider only flexural modes of the cantilever and normal out-of-plane oscillations for the sample surface as indicated in Fig.1. The displacement of the cantilever tip is η_c and the normal displacement of the sample surface is η_s. The quiescent, equilibrium distance between the cantilever tip and the sample surface in the presence of an interaction force is z_0. The tip-surface separation distance at an arbitrary time, when the cantilever or sample surface or both are in oscillation in the presence of the interaction force, is z. The spring model representing the dynamics of the tip-surface interaction is also shown in Fig.1. Both the cantilever and sample surface springs are assumed to be linear with stiffness constants k_{cn} and k_s, respectively, while the nonlinear interaction forces are represented by a nonlinear spring having a linear stiffness constant F' and a nonlinear stiffness constant F'' as indicated in the figure.

When the cantilever tip is in contact with the sample surface, the nonlinear tip-surface interaction force $F(z)$ provides a coupling of the cantilever and surface oscillations. The dynamics may be represented by a set of coupled differential equations for each mode n as

$$m_c\ddot{\eta}_{cn} + \gamma_c\dot{\eta}_{cn} + k_{cn}\eta_{cn} = F(z) + F_c\cos\omega_c t \tag{2}$$

$$m_s\ddot{\eta}_{sn} + \gamma_s\dot{\eta}_{sn} + k_s\eta_{sn} = F(z) + F_s\cos(\omega_s t + \theta) \tag{3}$$

where η_{cn} (positive down) is the cantilever tip displacement for mode n, η_{sn} (positive up) is the sample surface displacement for mode n, ω_c is the angular frequency of the cantilever oscillations, ω_s is the angular frequency of the sample surface vibrations, γ_c is the damping coefficient for the cantilever, γ_s is the damping coefficient for the sample surface, F_c is the magnitude of the cantilever driving force, F_s is the magnitude of the sample driving force that we assume here to result from an incident ultrasonic wave generated at the opposite surface of the sample, and θ is a phase contribution resulting from the propagation of the ultrasonic wave through the sample material.

We have shown previously[9] that for an acoustic wave propagating through a sample of thickness a/2 with phase velocity c and wave number k, containing an embedded feature of thickness d/2 for which the phase velocity is c_d, the total phase contribution θ is given by

$$\theta = -(\chi + \Delta\chi) \tag{4}$$

where

$$\chi = \frac{ka}{2} + \tan^{-1}\frac{\sin ka}{e^{\alpha a} - \cos ka} \quad , \tag{5}$$

$$\Delta\chi = -\psi\left[\frac{1}{2} + \frac{e^{\alpha a}\cos ka - 1}{(e^{\alpha a} - \cos ka)^2 + \sin^2 ka}\right] \quad , \tag{6}$$

and

$$\psi = kd\frac{(c_d - c)}{c_d} \quad . \tag{7}$$

The factor $-\chi$ is the contribution to the phase from the featureless bulk material and $-\Delta\chi$ is the contribution from a phase variation due to the embedded feature.

A typical nonlinear interaction force $F(z)$ is shown schematically in Fig.2. This force results from a number of possible fundamental mechanisms including electrostatic forces, van der Waals forces, interatomic repulsive (Born-Mayer) potentials, and Casimir forces[15]. It is also influenced by chemical potentials as well as hydroxyl bonds resulting from atmospheric moisture accumulation on the cantilever tip and sample surface[16].

We note from Fig.1 that for a given mode n, $z = z_o - (\eta_{cn} + \eta_{sn})$. We use this relationship in a power series expansion of $F(z)$ about z_o to obtain

$$F(z) = F(z_0) + F'(z_0)(z - z_0) + \frac{1}{2}F''(z_0)(z - z_0)^2 + \cdots \tag{8}$$

$$= F(z_0) - F'(z_0)(\eta_{cn} + \eta_{sn}) + \frac{1}{2}F''(z_0)(\eta_{cn} + \eta_{sn})^2 + \cdots$$

where the superscripted prime denotes derivative with respect to z. Substitution of Eq.(8) into Eqs.(2) and (3) gives

$$m_c\ddot{\eta}_{cn} + \gamma_c\dot{\eta}_{cn} + [k_{cn} + F'(z_0)]\eta_{cn} + F'(z_0)\eta_{sn} = F(z_0) + F_c\cos\omega_c t + \frac{1}{2}F''(z_0)(\eta_{cn} + \eta_{sn})^2 + \cdots \tag{9}$$

$$m_s\ddot{\eta}_{sn} + \gamma_s\dot{\eta}_{sn} + [k_s + F'(z_0)]\eta_{sn} + F'(z_0)\eta_{cn} = F(z_0) + F_s\cos(\omega_s t + \theta) + \frac{1}{2}F''(z_0)(\eta_{cn} + \eta_{sn})^2 + \cdots \ . \tag{10}$$

Equations (9) and (10) are the coupled equations representing the cantilever tip-sample surface dynamics resulting from the nonlinear interaction force at the sample surface.

B. Solution to general dynamical equations

We solve the coupled nonlinear Eqs.(9) and (10) for the steady-state solution by writing the coupled equations in matrix form and using a common iteration procedure to solve the matrix expression. The first iteration involves solving the equations for which the nonlinear terms are neglected. The second iteration is obtained by substituting the

first iterative solution into the nonlinear terms of Eqs.(9) and (10) and solving the resulting equations. The procedure provides solutions both for the cantilever tip and the sample surface displacements. Since the procedure is much too lengthy to reproduce here in full detail, only the salient features of the procedure leading to the steady state solution for the cantilever displacement $\eta_c = \sum \eta_{cn}$ are given. We begin by writing

$$\eta_{cn} = \varepsilon_{cn} + \xi_{cn} + \zeta_{cn} \tag{11}$$

and

$$\eta_{sn} = \varepsilon_{sn} + \xi_{sn} + \zeta_{sn} \tag{12}$$

where ε_{cn} and ξ_{cn} represent the first iteration (i.e. linear) static and oscillatory solutions, respectively, for the nth mode cantilever displacement, ζ_{cn} represents the second iteration (i.e., nonlinear) solution for the nth mode cantilever displacement, and ε_{sn} ,ξ_{sn}, and ζ_{sn} are the corresponding first and second iteration nth mode displacements for the sample surface.

i. First iterative solution

The first iterative solution is obtained by linearizing Eqs.(9) and (10), writing the resulting expression in matrix form, and solving the matrix expression assuming sinusoidal driving terms $F_c e^{i\omega_c t}$ and $F_s e^{i\omega_s t}$ for the cantilever and sample surface, respectively. The first iteration yields a static solution ε_{cn} and an oscillatory solution ξ_{cn} for the cantilever. The static solution is given by

$$\varepsilon_{cn} = \frac{k_s F(z_o)}{k_{cn}k_s + F'(z_o)(k_{cn} + k_s)} \quad . \tag{13}$$

The first iterative oscillatory solution is given by

$$\xi_{cn} = Q_{cc}\cos(\omega_c t + \alpha_{cc} - \phi_{cc}) + Q_{cs}\cos(\omega_s t - \phi_{ss} + \theta) \tag{14}$$

where

$$\phi_{cc} = \tag{15}$$

$$\tan^{-1}\frac{\omega_c(\gamma_s k_{cn} + \gamma_c k_s) - \omega_c^3(\gamma_s m_c + \gamma_c m_s) + F'(z_o)\omega_c(\gamma_s + \gamma_c)}{k_{cn}k_s + m_s m_c\omega_c^4 - \omega_c^2(m_s k_{cn} + m_c k_s + \gamma_c\gamma_s) + F'(z_o)(k_{cn} + k_s - m_s\omega_c^2 - m_c\omega_c^2)}$$

$$\phi_{ss} = \tag{16}$$

$$\tan^{-1}\frac{\omega_s(\gamma_s k_{cn} + \gamma_c k_s) - \omega_s^3(\gamma_s m_c + \gamma_c m_s) + F'(z_o)\omega_s(\gamma_s + \gamma_c)}{k_{cn}k_s + m_s m_c\omega_s^4 - \omega_s^2(m_s k_{cn} + m_c k_s + \gamma_c\gamma_s) + F'(z_o)(k_{cn} + k_s - m_s\omega_s^2 - m_c\omega_s^2)}$$

$$\begin{aligned} Q_{cc} = F_c\{&[k_s + F'(z_o) - m_s\omega_c^2]^2 + \gamma_s^2\omega_c^2\}^{1/2}\{[k_{cn}k_s + m_s m_c\omega_c^4 \\ &- \omega_c^2(m_s k_{cn} + m_c k_s + \gamma_c\gamma_s) + F'(z_o)(k_{cn} + k_s - m_s\omega_c^2 - m_c\omega_c^2)]^2 \\ &+ [\omega_c(\gamma_s k_{cn} + \gamma_c k_s) - \omega_c^3(\gamma_s m_c + \gamma_c m_s) + F'(z_o)\omega_c(\gamma_s + \gamma_c)]^2\}^{-1/2} \end{aligned} \tag{17}$$

and

$$Q_{cs} = -F_s F'(z_o)\{[k_{cn}k_s + m_s m_c\omega_s^4 - \omega_s^2(m_s k_{cn} + m_c k_s + \gamma_c\gamma_s)$$

$$+F'(z_o)(k_{cn}+k_s-m_s\omega_s^2-m_c\omega_s^2)]^2 \tag{18}$$

$$+[\omega_s(\gamma_s k_{cn}+\gamma_c k_s)-\omega_s^3(\gamma_s m_c+\gamma_c m_s)+F'(z_o)\omega_s(\gamma_s+\gamma_c)]^2\}^{-1/2}\ .$$

ii. Second iterative solution

The second iterative solution ζ_{cn} for each mode n of the cantilever is considerably more complicated, since it contains not only sum-frequency, difference-frequency, and harmonic-frequency components, but linear and static components as well. The second iterative solution ζ_{cn} is thus written as

$$\zeta_{cn}=\zeta_{cn,stat}+\zeta_{cn,lin}+\zeta_{cn,diff}+\zeta_{cn,sum}+\zeta_{cn,harm} \tag{19}$$

where $\zeta_{cn,stat}$ is a static or "dc" contribution generated by the nonlinear tip-surface interaction, $\zeta_{cn,lin}$ is a generated linear oscillatory contribution, $\zeta_{cn,diff}$ is a generated difference-frequency contribution resulting from the nonlinear mixing of the cantilever and sample oscillations, $\zeta_{cn,sum}$ is a generated sum-frequency contribution resulting from the nonlinear mixing of the cantilever and sample oscillations, and $\zeta_{cn,harm}$ are generated harmonic contributions.

Generally, the cantilever responds with decreasing displacement amplitudes as the drive frequency is increased above the fundamental resonance, even when driven at higher modal frequencies. Thus, acoustic-atomic force microscopy methods do not generally utilize harmonic or sum-frequency signals. For expediency, such signals from

the second iteration will not be considered here. Only the static, linear, and difference-frequency terms from the second iteration solution are relevant to currently-used A-AFM modalities.

The static contribution generated by the nonlinear interaction force is obtained to be

$$\zeta_{cn,stat} = \frac{1}{4}\frac{k_s F''(z_o)}{k_{cn}k_s + F'(z_o)(k_{cn}+k_s)}[2\varepsilon_o^2 + Q_{cc}^2 + Q_{cs}^2 + Q_{sc}^2 + Q_{ss}^2 + 2Q_{cc}Q_{sc}\cos(\alpha_{cc} - 2\phi_{cc}) + 2Q_{cs}Q_{ss}\cos\alpha_{ss}] \tag{20}$$

where

$$\varepsilon_o = \frac{(k_{cn}+k_s)F(z_o)}{k_{cn}k_s + F'(z_o)(k_{cn}+k_s)} \quad , \tag{21}$$

$$Q_{sc} = -F_c F'(z_o)\{[k_{cn}k_s + m_s m_c\omega_c^4 - \omega_c^2(m_s k_{cn} + m_c k_s + \gamma_c\gamma_s) + F'(z_o)(k_{cn} + k_s - m_s\omega_c^2 - m_c\omega_c^2)]^2 + [\omega_c(\gamma_s k_{cn} + \gamma_c k_s) - \omega_c^3(\gamma_s m_c + \gamma_c m_s) + F'(z_o)\omega_c(\gamma_s + \gamma_c)]^2\}^{-1/2} , \tag{22}$$

$$Q_{ss} = F_s\{[k_{cn} + F'(z_o) - m_c\omega_s^2]^2 + \gamma_c^2\omega_s^2\}^{1/2}\{[k_{cn}k_s + m_s m_c\omega_s^4 - \omega_s^2(m_s k_{cn} + m_c k_s + \gamma_c\gamma_s) + F'(z_o)(k_{cn} + k_s - m_s\omega_s^2 - m_c\omega_s^2)]^2 + [\omega_s(\gamma_s k_{cn} + \gamma_c k_s) - \omega_s^3(\gamma_s m_c + \gamma_c m_s) + F'(z_o)\omega_s(\gamma_s + \gamma_c)]^2\}^{-1/2} , \tag{23}$$

$$\alpha_{cc} = \tan^{-1} \frac{\gamma_s \omega_c}{k_s + F'(z_o) - m_s \omega_c^2} \quad , \tag{24}$$

$$\alpha_{ss} = \tan^{-1} \frac{\gamma_c \omega_s}{k_{cn} + F'(z_o) - m_c \omega_s^2} \quad , \tag{25}$$

and ϕ_{cc} is given by Eq.(15), Q_{cc} by Eq.(17) and Q_{cs} by Eq.(18).

The linear oscillatory contribution $\zeta_{cn,lin}$ generated by the nonlinear interaction force in the second iteration is obtained to be

$$\zeta_{cn,lin} = \frac{D_c}{R_{cc}} \varepsilon_o F''(z_o)[Q_{cc}^2 + Q_{sc}^2 + 2Q_{cc}Q_{sc}\cos\alpha_{cc}]^{1/2} \cos(\omega_c t - 2\phi_{cc} + \beta_c + \mu_{cc}) \tag{26}$$

$$+ \frac{D_s}{R_{ss}} \varepsilon_o F''(z_o)[Q_{ss}^2 + Q_{cs}^2 + 2Q_{ss}Q_{cs}\cos\alpha_{ss}]^{1/2} \cos(\omega_s t - 2\phi_{ss} + \beta_s + \mu_{ss} + \theta)$$

where

$$\mu_{cc} = \tan^{-1} \frac{Q_{cc}\sin\alpha_{cc}}{Q_{cc}\cos\alpha_{cc} + Q_{sc}} \quad , \tag{27}$$

$$\mu_{ss} = \tan^{-1} \frac{Q_{ss}\sin\alpha_{ss}}{Q_{ss}\cos\alpha_{ss} + Q_{cs}} \, , \tag{28}$$

$$\beta_c = \tan^{-1} \frac{\gamma_s \omega_c}{k_s - m_s \omega_c^2} \quad , \tag{29}$$

$$\beta_s = \tan^{-1} \frac{\gamma_s \omega_s}{k_s - m_s \omega_s^2} \quad , \tag{30}$$

$$D_c = [(k_s - m_s \omega_c^2)^2 + \gamma_s^2 \omega_c^2]^{1/2} \quad , \tag{31}$$

$$D_s = [(k_s - m_s \omega_s^2)^2 + \gamma_s^2 \omega_s^2]^{1/2} \quad , \tag{32}$$

$$R_{ss} = \{[k_{cn} k_s + m_s m_c \omega_s^4 - \omega_s^2 (m_s k_{cn} + m_c k_s + \gamma_c \gamma_s) + F'(z_o)(k_{cn} + k_s - m_s \omega_s^2 - m_c \omega_s^2)]^2$$

$$+ [\omega_s (\gamma_s k_{cn} + \gamma_c k_s) - \omega_s^3 (\gamma_s m_c + \gamma_c m_s) + F'(z_o) \omega_s (\gamma_s + \gamma_c)]^2\}^{1/2} \tag{33}$$

and

$$R_{cc} = \{[k_{cn} k_s + m_s m_c \omega_c^4 - \omega_c^2 (m_s k_{cn} + m_c k_s + \gamma_c \gamma_s) + F'(z_o)(k_{cn} + k_s - m_s \omega_c^2 - m_c \omega_c^2)]^2$$

$$+ [\omega_c (\gamma_s k_{cn} + \gamma_c k_s) - \omega_c^3 (\gamma_s m_c + \gamma_c m_s) + F'(z_o) \omega_c (\gamma_s + \gamma_c)]^2\}^{1/2} . \tag{34}$$

The difference-frequency contribution $\zeta_{cn,diff}$ generated by the nonlinear interaction force in the second iteration is obtained to be

$$\zeta_{cn,diff} = G_n \cos[(\omega_c - \omega_s)t - \phi_{cc} + \phi_{ss} + \beta_{cs} - \phi_{cs} + \Gamma - \theta] \tag{35}$$

where

$$G_n = \frac{1}{2}\frac{D_{cs}}{R_{cs}} F''(z_o)\{Q_{cc}^2 Q_{cs}^2 + Q_{sc}^2 Q_{ss}^2 + Q_{cc}^2 Q_{ss}^2 + Q_{cs}^2 Q_{sc}^2 \tag{36}$$

$$+ 2Q_{cc}Q_{cs}Q_{sc}Q_{ss}\cos(\alpha_{cc} + \alpha_{ss}) + 2Q_{cc}^2 Q_{cs}Q_{ss}\cos\alpha_{ss}$$

$$+ 2Q_{cc}Q_{cs}^2 Q_{sc}\cos\alpha_{cc} + 2Q_{sc}^2 Q_{ss}Q_{cs}\cos\alpha_{ss}$$

$$+ 2Q_{cc}Q_{ss}Q_{cs}Q_{sc}\cos(\alpha_{cc} - \alpha_{ss})\}^{1/2} \quad ,$$

$$D_{cs} = \sqrt{[k_s - m_s(\omega_c - \omega_s)]^2 + \gamma_s^2(\omega_c - \omega_s)^2} \quad , \tag{37}$$

$$R_{cs} = \sqrt{R_{cs1}^2 + R_{cs2}^2} \quad , \tag{38}$$

$$R_{cs1} = k_{cn}k_s - m_s k_{cn}(\omega_c - \omega_s)^2 - m_c k_s(\omega_c - \omega_s)^2 + m_s m_c(\omega_c - \omega_s)^4 \tag{39}$$

$$- \gamma_c\gamma_s(\omega_c - \omega_s)^2 + F'(z_o)[k_{cn} + k_s - m_s(\omega_c - \omega_s)^2 - m_c(\omega_c - \omega_s)^2] \ ,$$

$$R_{cs2} = (\omega_c - \omega_s)(\gamma_s k_c + \gamma_c k_s) - (\omega_c - \omega_s)^3(\gamma_s m_c + \gamma_c m_s) \tag{40}$$

$$+ F'(z_o)(\omega_c - \omega_s)(\gamma_s + \gamma_c) \ ,$$

$$\phi_{cs} = \tan^{-1}\frac{R_{cs2}}{R_{cs1}} \quad , \tag{41}$$

$$\beta_{cs} = \tan^{-1}\frac{\gamma_s(\omega_c - \omega_s)}{k_s - m_s(\omega_c - \omega_s)^2} \ , \tag{42}$$

and

$$\Gamma = \tan^{-1} \frac{Q_{cc}Q_{cs}\sin\alpha_{cc} - Q_{sc}Q_{ss}\sin\alpha_{ss} + Q_{cc}Q_{ss}\sin(\alpha_{cc} - \alpha_{ss})}{Q_{cc}Q_{cs}\cos\alpha_{cc} + Q_{sc}Q_{ss}\cos\alpha_{ss} + Q_{cc}Q_{ss}\cos(\alpha_{cc} - \alpha_{ss}) + Q_{cs}Q_{sc}} \quad . \quad (43)$$

iii. Salient features of the solution set

The total static solution to the coupled nonlinear equations (9) and (10) for the cantilever $\eta_{cn,stat}$ is the sum of the contribution ε_{cn}, given by Eq.(13), from the first iterative solution and the contribution $\zeta_{cn,stat}$, given by Eq.(20), from the second iteration as

$$\eta_{cn,stat} = \varepsilon_{cn} + \zeta_{cn,stat} \quad . \quad (44)$$

The total linear solution $\eta_{cn,lin}$ to Eqs.(9) and (10) is the sum of the contribution ξ_{cn} given by Eq.(14) and the contribution $\zeta_{cn,lin}$ given by Eq.(26) as

$$\eta_{cn,lin} = \xi_{cn} + \zeta_{cn,lin} \quad . \quad (45)$$

The total difference-frequency solution $\eta_{cn,diff}$ to Eqs.(9) and (10) is simply the contribution $\zeta_{cn,diff}$ given by Eq,(35).

It is interesting to note that ε_{cn} and the ε_o component in $\eta_{cn,stat}$ do not explicitly involve the cantilever drive amplitude F_c and the sample surface drive amplitude F_s, although other terms involving the Q factors, given by Eqs.(17), (18), (22),

and (23), in $\zeta_{cn,stat}$ do involve these drive amplitudes. This means that only the contributions stemming from the nonlinearity in the cantilever tip-sample surface interaction force respond directly to variations in the drive amplitudes and in particular to the physical features of the material giving rise to variations in F_s. Further, the magnitude of all second iteration (i.e. nonlinear) contributions, $\zeta_{cn,stat}$, $\zeta_{cn,lin}$, and $\zeta_{cn,diff}$ are strongly dependent on the cantilever tip-sample surface separation z_o, since the value of the nonlinear stiffness constant $F''(z_o)$ that dominates these contributions is highly sensitive to z_o. Indeed, $F''(z_o)$ attains a maximum value near the bottom of the force-separation curve of Fig.2.

It is interesting to note that the condition $k_{cn}k_s + F'(z_o)(k_{cn} + k_s) = 0$ gives a singularity in Eq.(13) for ε_{cn}, in Eq.(20) for $\zeta_{cn,stat}$, and in Eq.(26) [via ε_o of Eq.(21)] for $\zeta_{cn,lin}$. This condition on $F'(z_o)$ does not admit a solution to the original coupled Eqs.(9) and (10), since such a condition leads to a value of zero for the secular determinant of the coupled equations. On the other hand, the conditions $F'(z_o) = -k_{cn}$ or $F'(z_o) = -k_s$ do give rise to valid solutions to Eqs.(9) and (10) for all driving forces, static and non-static. The negative value of $F'(z_o)$ in this case means that the tip-surface separation distance z_o is smaller than the separation corresponding to that at the bottom (absolute minimum) of the force-separation curve. Eqs.(9) and (10) show that a negative value of $F'(z_o)$ reduces the effective magnitude of the stiffness constants both for the cantilever and the surface displacements. Indeed, the values $F'(z_o) = -k_{cn}$ and $F'(z_o) = -k_s$ give rise to effective null stiffness constants for the cantilever and surface

displacements, respectively, as indicated by the coefficients of η_{cn} and η_{sn} in Eqs.(9) and (10).

A further decrease in tip-surface separation z_o produces even larger negative values of $F'(z_o)$. From Eq.(9) we may define the effective cantilever resonance frequency for mode n as $\omega_{cn,eff} = \sqrt{[k_{cn} + F'(z_o)]/m_c}$. Thus, when $F'(z_o) < -k_{cn}$, $\omega_{cn,eff}$ becomes purely imaginary and produces an additional damping factor in the solutions to Eqs.(9) and (10). Such damping is reported by Rabe, Janser, and Arnold[17]. It is straightforward to obtain mathematically the effects of such an additional damping factor for the cantilever displacement amplitudes η_{cn}, if one considers only Eq.(9) and ignores the coupling term η_{sn}. For a driving force given by $F_c e^{i\omega_c t}$ the magnitude of the steady state solution to the equation is $|\eta_{cn}| = F_c\{[k_{cn} + F'(z_0) - m_c\omega_c^2]^2 + \gamma_c^2\omega_c^2\}^{-1/2}$. For a fixed drive frequency ω_c, effective cantilever mass m_c, and cantilever spring constant k_{cn}, the factor $F'(z_0)$ produces a decrease in the cantilever displacement amplitude $|\eta_{cn}|$ when $|F'(z_0)| > |k_{cn} - m_c\omega_c^2|$. Note that it matters little whether $F'(z_0)$ is positive or negative (i.e., whether z_0 is greater than or less than the value of z_0 at the bottom of the force-separation curve). As the cantilever is brought ever closer to the sample surface $F'(z_0)$ becomes ever larger in magnitude and $|\eta_{cn}|$ for each mode n continues to decrease until the repulsive force in the $F(z_o)$ curve of Fig.2 exceeds the fracture strength of the cantilever.

Finally, it is important to note that for large deflections of the cantilever that generally occur for hard contact (linear regime), large bending moments are introduced

that produce significant frequency shifts in the cantilever resonance frequencies quite apart from those introduced by the interaction force stiffness constant $F'(z_0)$. For the assessment of $F'(z_0)$ near the bottom of the force-separation curve where the nonlinearity $F''(z_0)$ is maximum (nonlinear regime) and $F'(z_0)$ is relatively small, a reasonable estimate of $F'(z_0)$ can be obtained directly from differences in the contact and non-contact resonance frequencies of the cantilever. For the assessment of $F'(z_0)$ in hard contact (linear regime) it is necessary to account for the bending moments of the cantilever in large deflection.

III. ESTIMATES OF PARAMETER MAGNITUDES

The results obtained in Section II are general equations of the cantilever response resulting from the cantilever tip-sample surface nonlinear force interaction. The equations are valid for all materials and material systems, including bio-materials. For many materials and microscope operating conditions, the general equations can be simplified by using estimates of the relative sizes of the parameters appearing in the equations. It is especially useful to obtain estimates of the order of magnitude of the parameters m_c, m_s, γ_c, γ_s, k_{cn}, and k_s that appear in the model. The estimates and resulting equation simplification are, of course, highly dependent on the particular material under investigation and on the specifications of the cantilever itself.

The cantilever stiffness constant k_{c1} corresponding to the fundamental mode (n = 1) oscillation is generally measured to lie in the range 0.02 – 80 N m^{-1}. A calculation of m_c can be obtained from measurements of the fundamental resonance angular frequency

of the cantilever in free space ω_{c1} and k_{c1} from the expression $m_c = k_{c1}/\omega_{c1}^2$. Measurements[17] of k_{c1} and ω_{c1} for typical commercial cantilevers indicate that m_c is of the order 10^{-11} - 10^{-12} kg.

We may obtain a crude estimate of m_s by noting that an oscillating cantilever tip in "point contact" with the sample surface generates spherical waves of frequency ω with pressure amplitude

$$p = \frac{P_o}{r} e^{i(\omega t - k_r r)} \tag{46}$$

where P_o is the pressure at unit radius, r is the radial distance from the contact point, and k_r is the radial wave number. We assume for definiteness that the "unit" radius is equal to the wave oscillation amplitude at the point of contact. Since "point contact" at the atomic level ideally involves an interaction between a single atom at the cantilever tip and a single atom of the sample surface, we assume that the wave displacement at the contact point corresponds to the relative motion between the two atoms. Assuming that the relative motion is of the order of interatomic distances, we estimate that the wave displacement amplitude is roughly 0.1 nm. From Eq.(46) we assume that when r = 100 "unit" radii, the magnitude of p is sufficiently small that the oscillating mass associated with such small pressures can be neglected. For a unit radius of 0.1 nm we obtain $r = 10^{-8}$ m. It is of interest to note that this value of r is in agreement with estimates[14] of the cantilever-sample contact radius r_c obtained from Hertzian contact theory using a contact force of 200 nN and a cantilever tip radius of 100 nm for a typical polymer material. The

hemispherical volume V of material corresponding to this radius is of the order 10^{-24} m^3. Assuming a mass density ρ of order 10^3 kg m^{-3} for the sample material (roughly a typical polymer density), we obtain $m_s = \rho V \approx 10^{-21}$ kg.

The magnitude of the sample stiffness constant k_s and the sample absorption coefficient γ_s can be estimated from the relationships of these parameters to the longitudinal elastic modulus and acoustic attenuation coefficient of the material, respectively. Consider a periodic solid lattice with lattice spacing L between lattice points of mass m. Let u_n represent the displacement of the nth lattice point from its equilibrium position resulting from a force F_n acting at that point. We assume that F_n is a function both of u_i and the particle velocity $\dot{u}_i$ where i takes the values n, n-1, and n+1. Hence, the force depends not only on the displacement and particle velocity of the nth lattice point but also on the displacements and particle velocities of points to either side of the nth point. Following the approach of reference 18 we may write from Newton's Law

$$m\frac{d^2u_n}{dt^2} = F_n = k_s[(u_{n+1} - u_n) - (u_n - u_{n-1})] + \gamma_s[(\dot{u}_{n+1} - \dot{u}_n) - (\dot{u}_n - \dot{u}_{n-1})] \qquad (47)$$

where k_s is the sample stiffness constant and γ_s is the sample or lattice absorption coefficient.

We divide Eq.(47) by AL = V, where A is some cross sectional area of the lattice and V is the volume enclosed by A and L. Taking the continuum limit as L approaches zero, we obtain the wave equation

$$\frac{\partial^2 u}{\partial t^2} = c^2 \frac{\partial^2 u}{\partial x^2} + \lambda_{dis} \frac{\partial^3 u}{\partial t \partial x^2} \tag{48}$$

where $c = (C_{11}/\rho)^{1/2}$ is the sound velocity, ρ = m/AL is the mass density of the material, $C_{11} = k_s L/A$ is the longitudinal elastic modulus, and $\lambda_{dis} = \gamma_s L/\rho A$ is the damping or dissipation coefficient for the continuous wave. The magnitude of k_s may be estimated from the relation $k_s = C_{11} A/L$ where A is the surface area subtended by the above-considered hemisphere of radius r. Assuming $C_{11} \approx 10^9$-10^{11} Pa, $r \approx 10^{-8}$ m, and $L \approx 0.4$ nm, we obtain $k_s \approx (10^2 - 10^4)$ N m^{-1}.

We may estimate the magnitude of γ_s by assuming a solution to Eq.(48) of the form $u = u_0 e^{i(kx-\omega t)}$ where k is a complex wave number. Substituting this form into Eq.(48), we obtain $k^2 = (\omega/c)^2[1 - i(\omega\lambda_{dis}/c^2]^{-1}$. The imaginary part of k is the acoustic attenuation coefficient α from which we obtain

$$\gamma_s = \frac{2S\rho c^3 \alpha}{L\omega^2} \quad . \tag{49}$$

An examination of the attenuation coefficients of a variety of materials in both the liquid and solid states together with other parameters occurring in Eq.(49) reveals that the magnitude of γ_s for most materials falls in the range $10^{-4} - 10^{-7}$ kg s^{-1}.

IV. APPLICATION OF MODEL TO VARIOUS ACOUSTIC-ATOMIC FORCE MICROSCOPE TECHNIQUES

The estimate of parameters obtained in Section III may be used to simplify the equations derived in Section II describing the cantilever response resulting from the interaction with the nonlinear cantilever tip-sample surface forces. The specific simplification depends on the particular acoustic-atomic force microscopy under consideration, the frequencies employed, and the material under investigation. We shall consider the most frequently used A-AFM modalities including resonant difference-frequency atomic force ultrasonic microscopy (RDF-AFUM), heterodyne force microscopy (HFM), ultrasonic force microscopy (UFM), atomic force acoustic microscopy (AFAM), force modulation microscopy (FMM), and the most commonly used intermittent contact mode.

A. Resonant difference-frequency atomic force ultrasonic microscopy and heterodyne force microscopy

Resonant difference-frequency atomic force ultrasonic microscopy (RDF-AFUM) employs an ultrasonic wave launched from the bottom of a sample, while the cantilever of an atomic force microscope, driven at a frequency differing from the ultrasonic frequency by one of the contact resonance frequencies of the cantilever, engages the sample top surface. It is important to note that at high drive amplitudes of the ultrasonic wave or cantilever (or both) the contact resonance frequency generating the difference-frequency signal may correspond to one of the nonlinear oscillation modes of the cantilever. As pointed out in Section II.B.*iii*, the effective contact cantilever resonance

frequency for the (linear or nonlinear) mode n, $\omega_{cn,eff}$, may be defined as $\omega_{cn,eff} = \sqrt{[k_{cn} + F'(z_o)]/m_c}$, where k_{cn} is the cantilever stiffness constant corresponding to the nth (linear or nonlinear) non-contact resonance mode. Since $F'(z_0)$ is negative at the separation distance z_0 corresponding to the maximum nonlinearity, i.e. maximum $F''(z_0)$, the resonance frequency of the cantilever in contact is smaller than the value when not in contact. The nonlinear mixing of the oscillating cantilever and the ultrasonic wave in the region defined by the cantilever tip-sample surface interaction force generates difference-frequency oscillations at the cantilever contact (linear or nonlinear) resonance.

Variations in the amplitude and phase of the bulk wave due to the presence of subsurface nano/microstructures as well as variations in near-surface material parameters affect the amplitude and phase of the difference-frequency signal. These variations are used to create spatial mappings generated by subsurface and near-surface structures. Heterodyne force microscopy (HFM) also utilizes difference-frequency signals generated by the nonlinear mixing in the cantilever tip-sample surface interaction region. In this technique no special advantage is taken of cantilever resonances and the difference-frequency utilized is generally well below that of the cantilever resonance.

In both RDF-AFUM and HFM the cantilever difference-frequency response is obtained from the nonlinear mixing in the region defined by the tip-surface interaction force. The interaction force varies nonlinearly with the tip-surface separation distance. The deflection of the cantilever obtained in calibration plots is related to this force; for small slopes of the deflection versus separation distance, the interaction force and cantilever deflection curves are approximately related via a constant of proportionality.

The maximum difference-frequency signal amplitude occurs when the quiescent deflection of the cantilever approaches the bottom of the force well, where the maximum change in the slope of the force versus separation curve (hence maximum interaction force nonlinearity) occurs.

The dominant term or terms for the cantilever difference-frequency displacement in Eqs.(1) and (11) depend on the values of k_{cn} both for the linear and the nonlinear non-contact modes of cantilever oscillation, $\Delta\omega$, and the value of $F'(z_0)$ obtained at the separation distance z_0 at which the maximum difference-frequency signal occurs. We designate the non-contact linear or nonlinear mode n for which the difference-frequency contact resonance occurs as n = p. The dominant difference-frequency component in Eqs.(1) and (11) is thus $\eta_{cp} = \eta_{cp,diff} = \zeta_{cp,diff}$ and is given by Eq.(35) for n = p as

$$\zeta_{cp,diff} = G_p \cos[(\omega_c - \omega_s)t - \phi_{cc} + \phi_{ss} + \beta_{cs} - \phi_{cs} + \Gamma - \theta] \quad . \tag{50}$$

where G_p, given by Eq.(36), and the phase terms in Eq.(50) are obtained from Eqs.(15)-(18), (21)-(25), (37)-(43). It is important to point out in considering these equations that while the difference-frequency resonance frequency $(\omega_c - \omega_s)$ in RDF-AFUM is usually set to correspond to the lowest contact resonance mode of the cantilever (although a higher modal resonance could be used), the cantilever driving frequency ω_c and ultrasonic frequency ω_s generally are set near (but not necessary equal to) higher contact resonance modes n = q and n = r , respectively, of the cantilever. For relatively small difference-frequencies, it may occur that q = r. Thus, the cantilever stiffness constant k_{cn}

is appropriately given as k_{cp} when involving the difference-frequency terms in Eqs.(15)-(18), (21)-(25), (37)-(43), the stiffness constant k_{cq} when involving the cantilever drive frequency ω_c at or near the frequency of the qth cantilever resonance mode, and k_{cr} when involving the ultrasonic frequency ω_s at or near the frequency of the rth cantilever resonance mode. If ω_c and ω_s are not set at or near a contact resonance modal frequency of the cantilever, then it may be necessary to include more than one term in Eq.(1) and (11) corresponding to different values of q and r.

It is seen from Eq.(36) that for a given value of $(\omega_c - \omega_s)$ the maximum value of $\zeta_{cp,diff}$ ideally occurs for a value of z_0 such that $F''(z_0)$ is maximized. An examination of the force-separation curve of Fig.2 suggests that $F''(z_0)$ is maximized near the bottom of the curve. It is important to note, however, that $F'(z_0)$, while relatively small compared to that of the hard contact regime, is generally not equal to zero at that point. Strictly, the values of $F''(z_0)$ and $F'(z_0)$ for a given z_0 are each dependent on the exact functional form of $F(z_0)$. A functional form for $F(z_0)$ sufficiently quantitative to quantify $F''(z_0)$ and $F'(z_0)$ is not typically available. However, experimental curves for $F(z_0)$ can be obtained and compared[9] to the experimental curves of $\zeta_{cp,diff}$ plotted as a function of z_0. It is generally found that for a given difference-frequency $(\omega_c - \omega_s)$ the maximum value of $\zeta_{cp,diff}$ occurs when $F'(z_0)$ is negative, that is when z_0 is slightly smaller than the value of z_0 corresponding to the minimum value of $F(z_0)$ in Fig.2. An examination of Eq.(36) suggests that a more exact approach to maximizing $\zeta_{cp,diff}$ would be not only to vary z_0 but also to vary slightly the difference-frequency

from the free space resonance condition until an optimal setting for both z_0 and the difference-frequency is achieved.

The equations for G_p and the phase terms in Eq.(50) may be simplified by using the values of the parameters estimated in Section III. All terms in Eqs.(15)-(18), (21)-(25), (37)-(43) involving the sample mass m_s may be dropped to an excellent approximation. For ultrasonic wave and the cantilever drive frequencies in the low megahertz range we obtain, setting $\Delta\omega = (\omega_c - \omega_s)$, that

$$\beta_{cs} \approx \tan^{-1} \frac{\gamma_s(\Delta\omega)}{k_s} \quad , \tag{51}$$

$$\phi_{cs} \approx \tan^{-1} \frac{(\gamma_c k_s + \gamma_s k_{cp})(\Delta\omega) - \gamma_s m_c (\Delta\omega)^3 + F'(z_0)(\gamma_c + \gamma_s)(\Delta\omega)}{k_{cp}k_s - (m_c k_s + \gamma_c\gamma_s)(\Delta\omega)^2 + F'(z_0)[k_{cp} + k_s - m_c(\Delta\omega)^2]} \quad , \tag{52}$$

$$\phi_{cc} \approx \tan^{-1} \frac{(\gamma_c k_s + \gamma_s k_{cq})\omega_c - \gamma_s m_c \omega_c^3 + F'(z_0)(\gamma_c + \gamma_s)\omega_c}{k_{cq}k_s - (m_c k_s + \gamma_c\gamma_s)\omega_c^2 + F'(z_0)(k_{cq} + k_s - m_c\omega_c^2)} \quad , \tag{53}$$

$$\phi_{ss} \approx \tan^{-1} \frac{(\gamma_c k_s + \gamma_s k_{cr})\omega_s - \gamma_s m_c \omega_s^3 + F'(z_0)(\gamma_c + \gamma_s)\omega_s}{k_{cr}k_s - (m_c k_s + \gamma_c\gamma_s)\omega_s^2 + F'(z_0)(k_{cr} + k_s - m_c\omega_s^2)} \quad , \tag{54}$$

and G_p is given by Eq.(36) where

$$\frac{D_{cs}}{R_{cs}} \approx \{[k_s^2 + \gamma_s^2(\Delta\omega)^2\}^{1/2}\{[k_{cp}k_s - (\Delta\omega)^2(m_c k_s + \gamma_c\gamma_s)$$

$$+ F'(z_o)(k_{cp} + k_s - m_c(\Delta\omega)^2)]^2 \qquad (55)$$

$$+ [(\Delta\omega)(\gamma_s k_{cp} + \gamma_c k_s) - (\Delta\omega)^3\gamma_s m_c + F'(z_o)\omega_c(\gamma_s + \gamma_c)]^2\}^{-1/2} \ ,$$

$$Q_{cc} \approx F_c\{[k_s + F'(z_o)]^2 + \gamma_s^2\omega_c^2\}^{1/2}\{[k_{cq}k_s$$

$$- \omega_c^2(m_c k_s + \gamma_c\gamma_s) + F'(z_o)(k_{cq} + k_s - m_c\omega_c^2)]^2 \qquad (56)$$

$$+ [\omega_c(\gamma_s k_{cq} + \gamma_c k_s) - \omega_c^3\gamma_s m_c + F'(z_o)\omega_c(\gamma_s + \gamma_c)]^2\}^{-1/2} \ ,$$

$$Q_{ss} \approx F_s\{[k_s + F'(z_o)]^2 + \gamma_s^2\omega_s^2\}^{1/2}\{[k_{cr}k_s$$

$$- \omega_s^2(m_c k_s + \gamma_c\gamma_s) + F'(z_o)(k_{cr} + k_s - m_c\omega_s^2)]^2 \qquad (57)$$

$$+ [\omega_s(\gamma_s k_{cr} + \gamma_c k_s) - \omega_s^3\gamma_s m_c + F'(z_o)\omega_c(\gamma_s + \gamma_c)]^2\}^{-1/2} \ ,$$

$$Q_{cs} \approx -F_s F'(z_o)\{[k_{cr}k_s - \omega_s^2(m_c k_s + \gamma_c\gamma_s) + F'(z_o)(k_{cr} + k_s - m_c\omega_s^2)]^2 \qquad (58)$$

$$+ [\omega_s(\gamma_s k_{cr} + \gamma_c k_s) - \omega_s^3\gamma_s m_c + F'(z_o)\omega_s(\gamma_s + \gamma_c)]^2\}^{-1/2} \ ,$$

and

$$Q_{sc} \approx -F_c F'(z_o)\{[k_{cq}k_s - \omega_c^2(m_c k_s + \gamma_c\gamma_s) + F'(z_o)(k_{cq} + k_s - m_c\omega_c^2)]^2 \qquad (59)$$

$$+[\omega_c(\gamma_s k_{cq}+\gamma_c k_s)-\omega_c^3\gamma_s m_c+F'(z_o)\omega_c(\gamma_s+\gamma_c)]^2\}^{-1/2}.$$

The phase term Γ in Eq.(50) is given by Eq.(43) and is quite complicated. However, advantage can be taken of the fact that k_s is generally quite large compared to other terms in the numerators of Q_{cc}, Q_{ss}, Q_{cs}, and Q_{sc}; the denominators of these terms are very roughly all equal. Hence, the magnitudes of Q_{cc} and Q_{ss} are usually quite large compared to those of Q_{cs} and Q_{sc}. The terms involving the product $Q_{cc}Q_{ss}$ thus dominate in Eq.(43) and we may approximate Γ as

$$\Gamma \approx \alpha_{cc}-\alpha_{ss}=\tan^{-1}\frac{\gamma_s\omega_c}{k_s+F'(z_0)}-\tan^{-1}\frac{\gamma_c\omega_s}{k_{cr}+F'(z_0)-m_c\omega_s^2} \tag{60}$$

where α_{cc} and α_{ss} are obtained from Eqs.(24) and (25), respectively. To the same extent that Γ may be approximated by Eq.(60) we may approximate G_p as

$$G_p \approx \frac{F''(z_0)}{2}\frac{D_{cs}}{R_{cs}}Q_{cc}Q_{ss} \quad . \tag{61}$$

It is seen from Eqs.(50)-(61) that both the amplitude and phase of the difference-frequency signal $\zeta_{cp,diff}$ are dependent on F_s, F_c, k_s, k_c, γ_s, and γ_c in addition to ω_c and ω_s. Since k_s is proportional to the Young modulus of the material, the dependence of $\zeta_{cp,diff}$ on γ_s and k_s means that scans of the sample contain information about the elastic stiffness of the sample as well as information about surface damping, hence viscoelastic

properties of the sample surface. Subsurface features of the sample are obtained via the dependence of the difference-frequency signal amplitude on F_s and via the dependence of the difference-frequency phase signal on θ, since both F_s and θ vary as the result of ultrasonic wave scattering from subsurface features. The signal response for HFM is generally given by the same equations as those for RDF-AFUM except that a single mode p may not necessarily dominate the signal, if the difference-frequency is above the lowest contact resonance frequency of the cantilever. A sum of the largest modal contributions is thus calculated for HFM to obtain the signal output. However, the difference-frequency in HFM generally is set well below the lowest contact modal frequency of the cantilever. In this case the appropriate equations are identical to those of RDF-AFUM with p equal to the lowest linear or nonlinear contact modal frequency of the cantilever.

B. Ultrasonic force microscopy

In ultrasonic force microscopy (UFM) the cantilever drive frequency ω_c and drive amplitude F_c are zero; the surface drive amplitude F_s and the drive frequency ω_s of the wave generated by the transducer at the bottom of the sample are nonzero. UFM can be operated at quite large frequencies, even in the gigahertz range. Although the vibrational response of the cantilever is certainly quite small at such frequencies, operation at a tip-surface separation distance z_0 corresponding to the nonlinear regime of the force-separation curve, where $F''(z_0)$ is maximum, will produce a detectable static or "dc" signal from the interaction nonlinearity. The generated static signal is called the ultrasonic force.

The nonlinear force-separation interaction results in a static displacement of the cantilever $\eta_{c,stat}$ given as

$$\eta_{c,stat} = \sum_n \eta_{cn,stat} \tag{62}$$

where $\eta_{cn,stat}$ is the contribution from mode n given by

$$\eta_{cn,stat} = \varepsilon_{cn} + \zeta_{cn,stat} \tag{63}$$

and ε_{cn} and $\zeta_{cn,stat}$ are given by Eqs.(13) and (20), respectively. Terms in Eq.(20) involving Q_{cc} and Q_{sc} are zero, since F_c is zero for UFM. We assume operation of the UFM in the nonlinear regime where $F''(z_0)$ is maximized and $F'(z_0)$ is negative. Using the values of the parameters estimated in Section III in the megahertz range of frequencies, we may approximate the nonzero terms Q_{ss} and Q_{cs} in Eq.(20) by Eqs.(57) and (58), where k_{cq} is replaced with k_{cn}. We obtain

$$\eta_{cn,stat} = \frac{k_s}{k_{cn}k_s + F'(z_o)(k_{cn} + k_s)}\{F(z_0) + \frac{F''(z_0)}{4}[2\varepsilon_o^2 + Q_{cs}^2 + Q_{ss}^2 + 2Q_{cs}Q_{ss}\cos\alpha_{ss}]\} \tag{64}$$

where ε_0 is given by Eq.(21) and α_{ss} is given by Eq.(25). To the extent that Q_{ss} is much larger than Q_{cs} because of the occurrence of k_s and $\gamma_s\omega_s$ in the numerator of Q_{ss}, Eq.(64) may be simplified by dropping the terms involving Q_{cs}.

Eq.(62) admits all cantilever modes as contributors to the magnitude of the UFM signal. However, Eq.(64) shows that the contribution to $\eta_{c,stat}$ for a given mode n is dependent on k_{cn} such that for both the ultrasonic and non-oscillatory contributions to Eq.(64) an increase in k_{cn} results in a decrease in the magnitude of the contributions for that mode. Since k_{cn} increases in magnitude with increasing n, the contribution to $\eta_{c,stat}$ from a given mode generally decreases with increasing mode number for both the ultrasonic and non-oscillatory components of $\eta_{cn,stat}$, although the exact relationship is highly dependent on the values of γ_c, γ_s, k_s, m_c, and ω_s that appear in Eq. (64).

The dominant contributions from the second term on the right-hand side of Eq.(64) for a given ultrasonic drive frequency ω_s occur for those cantilever modes having values of $[k_{cn} + F'(z_0)]$ near the value $m_c\omega_s^2$. The largest contributions occur for values of ω_s near a contact modal resonance frequency of the cantilever $\sqrt{[k_{cn} + F'(z_0)]/m_c}$. In contrast, the first term on the right-hand side of Eq.(64) and the component of the second term involving ε_0 are independent of frequency and thus make the major contributions when the ultrasonic drive frequencies are in the gigahertz range. These terms predict that a static signal exists even without the presence of an ultrasonic wave propagating through the sample and results directly from the interaction of the cantilever with the sample surface via the interaction force, as would be expected.

It is seen from Eq.(64) that $\eta_{cn,stat}$ is dependent on both F_s and k_s. This means that scans of the sample contain information about the elastic stiffness of the sample through k_s as well as information about subsurface features via the dependence of the amplitude on F_s. The dependence on γ_s means that UFM is sensitive to the viscous properties at the sample surface as well.

C. Atomic force acoustic microscopy and force modulation microscopy

Both for atomic force acoustic microscopy (AFAM) and force modulation microscopy (FMM) the cantilever drive amplitude and frequency are zero. As in UFM, the surface drive amplitude and frequency ω_s are nonzero. However, unlike UFM, the surface drive frequency is limited to a range of frequencies that produces measurable displacement amplitudes of cantilever oscillation. In contrast to UFM, the tip-surface interaction distance is set to operate in hard contact, the "linear detection regime" of operation, where z_0 is small, $F(z_0)$ is repulsive, $F'(z_0)$ is large and negative, and $F''(z_0)$ is negligible. In the "linear detection regime" no difference-frequency or harmonically generated signal is detectable, since for hard contact $F''(z_0)$ is effectively zero. The cantilever displacement amplitude $\eta_{cn,lin}$ corresponding to the nth mode is then obtained from Eq.(45) as $\eta_{cn,lin} = \varepsilon_{cn} + \zeta_{cn,lin}$. The contribution $\zeta_{cn,lin}$ resulting from the nonlinearity is given by Eq.(26) and is seen to be zero, since $F''(z_0)$ is effectively zero in the "linear detection regime." The remaining contribution ε_{cn} to the cantilever displacement amplitude is given by Eq.(14). For values of the parameters

estimated in Section III we may approximate ε_{cn}, hence $\eta_{cn,lin}$, in the low megahertz range of frequencies as

$$\eta_{cn,lin} \approx \varepsilon_{cn} \approx Q_{cs}\cos(\omega_s t - \phi_{ss} + \theta) \tag{65}$$

where Q_{cs} is given by Eq.(58), ϕ_{ss} by Eq.(54), and θ .by Eq.(4).

Note that both Q_{cs} and ϕ_{ss} depend on the magnitude of $F'(z_0)$. For sufficiently hard contact $F'(z_0)$ becomes very large and negative and may dominate the terms in Eq.(65). Under such conditions we obtain

$$Q_{cs} \approx -F_s\{(k_{cn} + k_s - m_c\omega_s^2)^2 + (\gamma_c + \gamma_s)^2\omega_s^2\}^{-1/2} \tag{66}$$

and

$$\phi_{ss} \approx \tan^{-1}\frac{(\gamma_c + \gamma_s)\omega_s}{k_{cn} + k_s - m_c\omega_s^2} \quad . \tag{67}$$

Eqs.(65)-(67) show that both the amplitude and phase of the cantilever oscillations depend on k_{cn}, k_s, γ_c, γ_s, and ω_s. For AFAM driving frequencies ω_s near a cantilever resonance $\sqrt{k_{cn}/m_c}$ corresponding to mode n, the signal amplitude is large and the cantilever displacement is dominated by that mode. Although Eqs.(66) and (67) appear to be independent of $F'(z_0)$, the equations are subtly dependent on $F'(z_0)$ via the restrictions $F'(z_0)$ places on the resonance modes available. As pointed out in Section II.B.*iii*, larges negative values of $F'(z_0)$ eliminate from consideration all modes for

which $F'(z_0) \leq -k_{cn}$. For FMM, ω_s is much smaller than $\sqrt{k_{c1}/m_c}$, the fundamental cantilever resonance frequency, although the fundamental resonance may not appear in the calculations if $F'(z_0) \leq k_{c1}$.

D. Intermittent contact mode

The intermittent contact mode (TappingMode) is a standard feature on many atomic force microscopes in which the cantilever is driven in oscillation, but no surface oscillations resulting from bulk ultrasonic waves are generated (i.e., F_s and ω_s are zero). Thus, the intermittent contact mode cannot be used to image subsurface features, but interesting surface properties and features can be imaged. Since intermittent contact mode can be used in both hard and soft tip-surface contact (i.e. the linear and nonlinear regimes, respectively, of the force-separation curve), the cantilever displacement $\eta_{cn,lin}$ for mode n is given most generally as

$$\eta_{cn.lin} = \xi_{cn} + \zeta_{cn,lin} \tag{68}$$

where ξ_{cn} is given by Eq.(14) with the term involving Q_{cs} set equal to zero and $\zeta_{cn,lin}$ is given by Eq.(26) with all terms involving Q_{cs} and Q_{ss} set equal to zero.

For the soft contact regime the expression for $\eta_{cn,lin}$ is

$$\eta_{cn,lin} = H\cos(\omega_c t - \phi_{cc} + \Lambda) \tag{69}$$

where

$$\Lambda = \tan^{-1} \frac{\sin(\beta_c + \mu_{cc} - \phi_{cc} - \alpha_{cc})}{\cos(\beta_c + \mu_{cc} - \phi_{cc} - \alpha_{cc}) + (Q_{cc}/W)} \quad , \tag{70}$$

$$W = \frac{D_c}{R_{cc}} \varepsilon_0 F''(z_0)(Q_{cc}^2 + Q_{sc}^2 + 2Q_{cc}Q_{sc}\cos\alpha_{cc})^{1/2} \quad , \tag{71}$$

and

$$H = [Q_{cc}^2 + W^2 + 2Q_{cc}W\cos(\beta_c + \mu_{cc} - \phi_{cc} - \alpha_{cc})]^{1/2} \tag{72}$$

where Q_{cc} is given by Eq.(56), Q_{sc} by Eq.(59), ϕ_{cc} by Eq.(53), μ_{cc} by Eq.(27), ε_0 by Eq.(21); a_{cc}, β_c, D_c, and R_{cc}, are given by Eqs.(24), (29), (31), and (34), respectively, with the terms involving m_s set equal to zero.

The complexity of the cantilever response $\eta_{cn,lin}$ is greatly reduced for the hard contact regime, where $F''(z_0)$ is negligibly small and $F'(z_0)$ is very large and negative. For hard contact Λ and α_{cc} are approximately zero and we obtain

$$\eta_{cn,lin} \approx Q_{cc}\cos(\omega_c t - \phi_{cc}) \tag{73}$$

where

$$Q_{cc} = F_c[(k_{cn} + k_s - m_c\omega_c^2)^2 + (\gamma_c + \gamma_s)^2\omega_c^2]^{-1/2} \tag{74}$$

and

$$\phi_{cc} = \tan^{-1} \frac{(\gamma_c + \gamma_s)\omega_c}{k_{cn} + k_s - m_c\omega_c^2} \quad . \tag{75}$$

The dependence of $\eta_{cn,lin}$ on the material damping coefficient γ_s and the sample stiffness constant k_s, both for the hard and the soft contact regimes, means that the intermittent contact mode can be used to assess the viscoelastic properties of the material irrespective of the regime of operation.

V. IMAGE CONTRAST

All the above equations, except for Eqs.(4) and (6), were derived for constant values of the cantilever and material parameters. If, in an area scan of the sample, the parameters remain constant from point to point, the image generated from the scan would be flat and featureless. We consider here that the sample stiffness constant k_s may vary from point to point on the sample surface. Since k_s is proportional to the Young modulus E, this means that E also varies from point to point. We assume that the value of the sample stiffness constant k_s' at a given point on the surface differs from the value k_s at another position as $k_s' = k_s + \Delta k_s$. For any function $f(k_s)$ having a functional dependence on k_s, a variation in k_s generates a variation in $f(k_s)$ given as $\Delta f = (df/dk_s)_0 \Delta k_s$, where the subscripted zero indicates evaluation at k_s. A similar expression can be obtained for the material damping parameter γ_s, but we shall not consider such variations here.

A variation in k_s produces a variation both in the amplitude and phase of the signal generated by the cantilever tip-sample surface interactions. The variations in amplitude and phase can be used to generate amplitude and phase images, respectively, in

a surface scan of the sample. We first consider images generated by the phase variations in the signal.

A. Phase-generated images

The phase factors involved in RDF-AFUM and HFM are given from Eq.(50), (4), and (5) to be ϕ_{cc}, ϕ_{ss}, β_{cs}, ϕ_{cs}, Γ, and χ; the phase factors involved in AFAM and FMM are, from Eq.(65), ϕ_{ss} and χ; the phase factors involved in the intermittent contact mode are, from Eq.(69), ϕ_{cc}, and Λ. Each of these phase factors is dependent on k_s and the variations in the phase factors resulting from variations in k_s are responsible for image generation when using phase detection of the A-AFM signal. The exact dependence of the phase on k_s, however, is different for soft and hard contact regimes.

i. Soft contact regime

For the soft contact regime the appropriate variations in the phase factors relevant to HFM and RDF-AFUM are

$$\Delta\beta_{cs} = \left(\frac{d\beta_{cs}}{dk_s}\right)_0 \Delta k_s = -\frac{\gamma_s \Delta\omega}{[k_s + F'(z_0)]^2 + \gamma_s^2(\Delta\omega)^2}\Delta k_s \quad , \tag{76}$$

$$\Delta\phi_{cc} = -\frac{A_{cc}}{B_{cc}}\Delta k_s \tag{77}$$

where

$$A_{cc} = [\gamma_s k_{cq}^2 + 2F'(z_0)\gamma_s k_{cq} + F'(z_0)^2(\gamma_c + \gamma_s)]\omega_c \tag{78}$$

$$+[\gamma_c^2\gamma_s - 2\gamma_s m_c(k_{cq} + F'(z_0)]\omega_c^3 + m_c^2\gamma_s\omega_c^5$$

and

$$B_{cc} = \{[\gamma_c k_s + \gamma_s k_{cq} + F'(z_0)(\gamma_c + \gamma_s)]\omega_c - \gamma_s m_c\omega_c^3\}^2 \tag{79}$$

$$+\{[k_{cq} - m_c\omega_c^2 + F'(z_0)]k_s + F'(z_0)(k_{cq} - m_c\omega_c^2) - \gamma_c\gamma_s\omega_c^2\}^2 \ ,$$

$$\Delta\phi_{ss} = -\frac{A_{ss}}{B_{ss}}\Delta k_s \tag{80}$$

where

$$A_{ss} = [\gamma_s k_{cr}^2 + 2F'(z_0)\gamma_s k_{cr} + F'(z_0)^2(\gamma_c + \gamma_s)]\omega_s \tag{81}$$

$$+[\gamma_c^2\gamma_s - 2\gamma_s m_c(k_{cr} + F'(z_0)]\omega_s^3 + m_c^2\gamma_s\omega_s^5$$

and

$$B_{ss} = \{[\gamma_c k_s + \gamma_s k_{cr} + F'(z_0)(\gamma_c + \gamma_s)]\omega_s - \gamma_s m_c\omega_s^3\}^2 \tag{82}$$

$$+\{[k_{cr} - m_c\omega_s^2 + F'(z_0)]k_s + F'(z_0)(k_{cr} - m_c\omega_s^2) - \gamma_c\gamma_s\omega_s^2\}^2 \ ,$$

and

$$\Delta\phi_{cs} = -\frac{A_{cs}}{B_{cs}}\Delta k_s \tag{83}$$

where

$$A_{cs} = [\gamma_s k_{cp}^2 + 2F'(z_0)\gamma_s k_{cp} + F'(z_0)^2(\gamma_c + \gamma_s)](\Delta\omega) \tag{84}$$

$$+[\gamma_c^2\gamma_s - 2\gamma_s m_c(k_{cp} + F'(z_0)](\Delta\omega)^3 + m_c^2\gamma_s(\Delta\omega)^5$$

and

$$B_{cs} = \{[\gamma_c k_s + \gamma_s k_{cp} + F'(z_0)(\gamma_c + \gamma_s)](\Delta\omega) - \gamma_s m_c(\Delta\omega)^3\}^2 \tag{85}$$

$$+\{[k_{cp}-m_c(\Delta\omega)^2+F'(z_0)]k_s+F'(z_0)[k_{cp}-m_c(\Delta\omega)^2]-\gamma_c\gamma_s(\Delta\omega)^2\}^2 \ .$$

To the extent that $\Gamma=\alpha_{cc}-\alpha_{ss}$, as given by Eq.(60), we may write

$$\Delta\Gamma=\Delta\alpha_{cc}=-\frac{\gamma_s\omega_c}{[k_s+F'(z_0)]^2+\gamma_s^2\omega_c^2}\Delta k_s \quad . \tag{86}$$

The phase term $\Delta\chi$ is given by Eqs.(6) and (7).

The appropriate variations in the phase factors relevant to the intermittent soft contact mode are $\Delta\alpha_{cc}$, $\Delta\phi_{cc}$, and $\Delta\Lambda$. The factor $\Delta\Lambda$ is obtained from Eq.(70) as

$$\Delta\Lambda=\frac{1+(Q_{cc}/W)\cos(\beta_c+\mu_{cc}-\phi_{cc}-\alpha_{cc})}{[\cos(\beta_c+\mu_{cc}-\phi_{cc}-\alpha_{cc})+(Q_{cc}/W)]^2+\sin^2(\beta_c+\mu_{cc}-\phi_{cc}-\alpha_{cc})} \tag{87}$$

$$\times(\Delta\beta_c+\Delta\mu_{cc}-\Delta\phi_{cc}-\Delta\alpha_{cc})$$

where

$$\Delta\beta_c=-\frac{\gamma_s\omega_c}{k_s^2+\gamma_s^2\omega_c^2}\Delta k_s \quad , \tag{88}$$

$\Delta\phi_{cc}$ is given by Eq.(77), and $\Delta\mu_{cc}$ is obtained from Eq.(27). To the extend that Q_{sc} is much smaller than Q_{cc}, we get from Eq.(27) that $\Delta\mu_{cc}=\Delta\alpha_{cc}$ where $\Delta\alpha_{cc}$ is given by Eq.(86).

ii. Hard contact regime

For the hard contact regime where $F'(z_0)$ is very large and negative, the relevant phase variations are obtained from Eqs.(67) and (75) as

$$\Delta\phi_{cc} = -\frac{(\gamma_c + \gamma_s)\omega_c}{(k_s + k_{cq} - m_c\omega_c^2)^2 + (\gamma_c + \gamma_s)^2\omega_c^2}\Delta k_s \quad , \tag{89}$$

and

$$\Delta\phi_{ss} = -\frac{(\gamma_c + \gamma_s)\omega_s}{(k_s + k_{cr} - m_c\omega_s^2)^2 + (\gamma_c + \gamma_s)^2\omega_s^2}\Delta k_s \quad . \tag{90}$$

Eqs.(89) and (90) are appropriate to AFAM and FMM modalities as well as to the intermittent hard contact mode of A-AFM operation.

iii. Dependence on the Young modulus

Hertzian contact theory provides that the sample stiffness constant k_s is related to the Young modulus E of the sample as[14]

$$k_s = 2r_c\left(\frac{1-\upsilon_T^2}{E_T} + \frac{1-\upsilon^2}{E}\right)^{-1} \tag{91}$$

where υ is the Poisson ratio of the sample material, E_T and υ_T are the Young modulus and Poisson ratio, respectively, of the cantilever tip, and r_c is the cantilever tip-sample surface contact radius. Hence,

$$\Delta k_s = \frac{2r_c\left(1-\upsilon^2\right)}{E^2}\left(\frac{1-\upsilon_T^2}{E_T}+\frac{1-\upsilon^2}{E}\right)^{-2}\Delta E \quad . \tag{92}$$

Eq.(92) can be used with Eqs(76)-(90) to ascertain the fractional variation in the Young modulus $\Delta E/E$ from measurements of the phase variation in the signal from an appropriate A-AFM modality.

B. Amplitude-generated images

The amplitude G_p of the RDF-AFUM signal is given by Eq.(61) to a good approximation for most applications. The fractional variation in the signal amplitude $\Delta G_p/G_p$ resulting from variations in the sample spring constant k_s, hence Young modulus E, makes a considerable contribution to the image contrast when operating in the amplitude detection modality. The fractional variation in amplitude is

$$\frac{\Delta G_p}{G_p} = \frac{1}{G_p}\left(\frac{\partial G_p}{\partial k_s}\right)_0 \Delta k_s$$

$$= \left\{\frac{1}{Q_{ss}}\left(\frac{\partial Q_{ss}}{\partial k_s}\right)_0 + \frac{1}{Q_{cc}}\left(\frac{\partial Q_{cc}}{\partial k_s}\right)_0 + \frac{R_{cs}}{D_{cs}}\left[\frac{\partial}{\partial k_s}\left(\frac{D_{cs}}{R_{cs}}\right)\right]_0\right\}\Delta k_s \tag{93}$$

where

$$\frac{1}{Q_{ss}}\left(\frac{\partial Q_{ss}}{\partial k_s}\right)_0 = \frac{k_s + F'(z_0)}{[(k_s + F'(z_0))^2 + c_{ss}^2]^{1/2}}$$

$$-\frac{(a_{ss}k_s + b_{ss})a_{ss} + (c_{ss}k_s + d_{ss})c_{ss}}{(a_{ss}k_s + b_{ss})^2 + (c_{ss}k_s + d_{ss})^2}, \tag{94}$$

$$a_{ss} = k_{cr} - m_c\omega_s^2 + F'(z_0) \quad , \tag{95}$$

$$b_{ss} = F'(z_0)(k_{cr} - m_c\omega_s^2) - \gamma_c\gamma_s\omega_s^2 \quad , \tag{96}$$

$$c_{ss} = \gamma_c\omega_s \quad , \tag{97}$$

$$d_{ss} = \gamma_s k_{cr}\omega_s - m_c\gamma_s\omega_s^3 + F'(z_0)(\gamma_c + \gamma_s) \quad ; \tag{98}$$

$$\frac{1}{Q_{cc}}\left(\frac{\partial Q_{cc}}{\partial k_s}\right)_0 = \frac{k_s + F'(z_0)}{[(k_s + F'(z_0))^2 + c_{cc}^2]^{1/2}}$$

$$-\frac{(a_{cc}k_s + b_{cc})a_{cc} + (c_{cc}k_s + d_{cc})c_{cc}}{(a_{cc}k_s + b_{cc})^2 + (c_{cc}k_s + d_{cc})^2}, \tag{99}$$

$$a_{cc} = k_{cq} - m_c\omega_c^2 + F'(z_0) \quad , \tag{100}$$

$$b_{cc} = F'(z_0)(k_{cq} - m_c\omega_c^2) - \gamma_c\gamma_s\omega_c^2 \quad , \tag{101}$$

$$c_{cc} = \gamma_c \omega_c \quad , \tag{102}$$

$$d_{cc} = \gamma_s k_{cq} \omega_c - m_c \gamma_s \omega_c^3 + F'(z_0)(\gamma_c + \gamma_s) \quad ; \tag{103}$$

and

$$\frac{R_{cs}}{D_{cs}}\left[\frac{\partial}{\partial k_s}\left(\frac{D_{cs}}{R_{cs}}\right)\right]_0 = \frac{k_s}{[(k_s^2 + c_{cs}^2]^{1/2}} \tag{104}$$

$$- \frac{(a_{cs}k_s + b_{cs})a_{ss} + (c_{cs}k_s + d_{cs})c_{cs}}{(a_{cs}k_s + b_{cs})^2 + (c_{cs}k_s + d_{cs})^2},$$

$$b_{cs} = k_{cp} - m_c(\Delta\omega)^2 + F'(z_0) \quad , \tag{105}$$

$$c_{cs} = F'(z_0)(k_{cp} - m_c(\Delta\omega)^2) - \gamma_c\gamma_s(\Delta\omega)^2 \quad , \tag{106}$$

$$d_{cs} = \gamma_c(\Delta\omega) \quad , \tag{107}$$

$$h_{cs} = \gamma_s k_{cp}(\Delta\omega) - m_c\gamma_s(\Delta\omega)^3 + F'(z_0)(\gamma_c + \gamma_s) \quad . \tag{108}$$

It is apparent from Eqs.(93)-(108) that, although the RDF-AFUM signal amplitude *per se* is highly dependent on $F''(z_0)$ and on the cantilever and ultrasonic drive amplitudes F_c and F_s, respectively, the magnitude of the fractional variation

$\Delta G_p / G_p$ in the RDF-AFUM signal amplitude resulting from variations in the sample spring constant k_s is independent of F_c, F_s, and $F''(z_0)$. However, $\Delta G_p / G_p$ is dependent upon the values of the cantilever spring constant k_{cn} where n = p, q, and r as discussed in Section IV.A. The values of k_{cn} in turn are highly dependent on the choice of cantilever and the frequency chosen to drive the cantilever into resonance. Although $\Delta G_p / G_p$ makes a considerable contribution to image contrast, it is not the only contribution. As with all A-AFM techniques the resolution of the image digitizer, the dynamic range and signal-to-noise features of the electronic components, the sharpness of the cantilever tip, and the bonding of the ultrasonic transducer among other factors also contribute to the image contrast. The contrast for RDF-AFUM, however, cannot generally exceed that rendered by $\Delta G_p / G_p$. The magnitude of the signal variation for HFM is given by the same equation as for RDF-AFUM except that a single mode may not necessary dominate the signal. A sum of the largest modal contributions may be appropriate to calculate for HFM the cantilever displacement.

The amplitude of the UFM signal is given by Eqs.(62)-(64). Assuming that Q_{cs} is small compared to Q_{ss} and ε_0, hence negligible in the calculations, we obtain the fractional variation in the cantilever displacement amplitude for the nth mode to be

$$\frac{\Delta\eta_{cn,stat}}{\eta_{cn,stat}} = \left\{ \frac{F'(z_0)k_{cn}}{k_s[k_{cn}k_s + F'(z_0)(k_{cn}+k_s)]} + \frac{F''(z_0)(\varepsilon_0 \frac{\partial \varepsilon_0}{\partial k_s} + \frac{1}{2} Q_{ss} \frac{\partial Q_{ss}}{\partial k_s})}{F(z_0) + \frac{F''(z_0)}{4}(2\varepsilon_0^2 + Q_{ss}^2)} \right\}_0 \Delta k_s \quad (109)$$

where Q_{ss} is given by Eq.(57) with q = n, $(\partial Q_{ss}/\partial k_s)_0$ by Eq.(94) with q = n, ε_0 by Eq.(21), and $(\partial \varepsilon_0/\partial k_s)_0$ by

$$\left(\frac{\partial \varepsilon_0}{\partial k_s}\right)_0 = -\frac{F(z_0)k_{cn}^2}{k_{cn}k_s + F'(z_0)(k_{cn}+k_s)} \quad . \tag{110}$$

For AFAM and FMM the cantilever displacement amplitude is from Eq.(65) dependent on Q_{cs} where Q_{cs} is given by Eq. (58). The fractional change in the signal amplitude for mode n is obtained to be

$$\frac{\Delta Q_{cs}}{Q_{cs}} = -\frac{k_{cn}+k_s-m_c\omega_s^2}{(k_{cn}+k_s-m_c\omega_s^2)+(\gamma_c+\gamma_s)^2\omega_s^2}\Delta k_s \quad . \tag{111}$$

The availability and dominance of modes are discussed in Section IV.C.

For the intermittent hard contact modality the amplitude is dependent on Q_{cc} which for hard contact is given by Eq.(74). The fractional change in the amplitude for a given mode n is obtained as

$$\frac{\Delta Q_{cc}}{Q_{cc}} = -\frac{k_{cn}+k_s-m_c\omega_c^2}{(k_{cn}+k_s-m_c\omega_c^2)+(\gamma_c+\gamma_s)^2\omega_c^2}\Delta k_s \quad . \tag{112}$$

It is interesting to note that the variation in amplitude for intermittent hard contact is identical to that of AFAM and FMM except that in intermittent hard contact the drive frequency is ω_c whereas in AFAM and FMM the drive frequency is ω_s.

VI. APPLICATION TO LARC-CP2 POLYIMIDE FILM

The above equations are applied to the assessment of $\Delta E/E$ in LaRC-cp2 polyimide polymer from measurements[9] of the variations in the phase signal using RDF-AFUM. The values of the relevant material and cantilever parameters are[9] k_s = 96.1 N m^{-1}, k_{c1} = 14 N m^{-1}, $\gamma_s = 4.8 \times 10^{-5}$ kg s^{-1}, $m_c = 3.9 \times 10^{-12}$ kg, E = 2.4 GPa, a/2 = 12.7 μm, α = 85 m^{-1}, $F'(z_0) = -53$, $\omega_c/2\pi$ = 2.1 MHz, $\omega_s/2\pi$ = 1.8 MHz, and $\Delta\omega/2\pi$ = 0.3 MHz. From Eq.(50) the variation in the phase signal is given as $(\Delta\phi_{ss} - \Delta\phi_{cc} + \Delta\beta_{cs} - \Delta\phi_{cs} + \Delta\Gamma + \Delta\chi)$. From Eqs.(6),(7),(76)-(86) we calculate that $\Delta\beta_{cs}$ and $\Delta\Gamma = \Delta\alpha_{cc}$ make by far the dominate contributions to the RDF-AFUM phase signal variations. The contribution from $\Delta\chi$ is relatively small because the thickness of the sample a/2 does not correspond to a resonance thickness for the ultrasonic wave. The factors $\Delta\phi_{ss}$ and $\Delta\phi_{cc}$ are relatively close in magnitude and result in relatively little net contribution to the phase variations in Eq.(50). The factor $\Delta\phi_{cs}$ is also calculated to be small with a sign opposite to that of $(\Delta\phi_{ss} - \Delta\phi_{cc})$ and results in further minimizing the net phase contribution from these three terms.

From the above equations and a measured phase variation of 13.2 degrees obtained in the RDF-AFUM phase image[9] we calculate a value of approximately 24 percent for the variation in the Young modulus for the material. This value is also in good agreement with a value of roughly 21 percent obtained from independent

mechanical stretching experiments in which the increase in the modulus is attributed to the growth during stretching of a crystalline phase having a larger Young modulus than that of the original amorphous phase[20]. The growth of the crystalline phase in LaRC-CP2 is attributed to internal stresses generated during curing by the different thermal expansion coefficients of the polymer material and gold nanoparticles embedded in the polymer matrix.

A further test of the present model can be obtained from the intermittent soft contact image taken concurrently with the RDF-AFUM image of the LaRC-CP2 specimen[9]. The variation in the phase signal is measured from the intermittent soft contact micrograph to be roughly 1.5 degrees. From Eq.(69) the variation in the phase signal for intermittent soft contact is analytically given as $(-\Delta\phi_{cc} + \Delta\Lambda)$. Using the above-stated values of the material and cantilever parameters in Eqs.(86)-(88) ,we calculate that for the measured variation of 1.5 degrees in the intermittent soft contact image the variation in the Young modulus is roughly 18 percent. This value is in good agreement with the values obtained from the RDF-AFUM image and from the independent, mechanical stretching measurements.

VII. CONCLUSION

The various modalities of acoustic-atomic force microscopy (A-AFM) have become important nanoscale characterization tools for the development of novel materials and devices. Most of the information obtained from A-AFM has been qualitative because of the lack of a comprehensive analytical model to render the data quantitative. The most significant impediment to the development of such a model has

been the nonlinearity of the cantilever tip-sample surface interaction force. We have developed a detailed mathematical model of this interaction by assuming that the interaction is appropriately represented by a nonlinear spring coupled at the opposite ends by linear springs representing simple harmonic oscillators for the cantilever and sample surface. The dynamics of the coupled springs are described by a pair of coupled differential equations that are solved using a standard iteration procedure. Only flexural vibrations of the cantilever and out-of-plane oscillations of the sample surface are considered in the present derivation.

Solutions are obtained for specific A-AFM modalities including the commonly used intermittent contact mode (TappingMode), force modulation microscopy (FMM), atomic force acoustic microscopy (AFAM), ultrasonic force microscopy (UFM), heterodyne force microscopy (HFM), and resonant difference-frequency atomic force ultrasonic microscopy (RDF-AFUM). Image generation and contrast equations are obtained for each of the aforementioned A-AFM modalities assuming for expediency that the contrast results only from variations in the sample stiffness constant. Since the sample stiffness constant is related directly to the Young modulus of the sample, the contrast can be expressed in terms of the variation in the Young modulus from point to point as the sample is scanned.

A portion of the present solution set was obtained previously[9] using feasibility arguments to render the analytical equations and applied to the assessment of the fractional variation in the Young modulus $\Delta E / E$ of LaRC^{TM}-CP2 polyimide polymer from measurements of the variations in the phase signal using RDF-AFUM. The present derivation provides a solid analytical framework for the feasibility arguments. The

calculation of 24 percent for $\Delta E/E$ is in good agreement with a value of 21 percent obtained from independent mechanical stretching experiments in which the increase in the modulus is attributed to the growth during stretching of a crystalline phase having a larger Young modulus than that of the original amorphous phase[20].

Further application of the model to intermittent soft contact images of the same polymer material yields a value of 18 percent for the variation of the Young modulus. This value is also in good agreement with the mechanical stretching experiments. The difference between the RDF-AFUM and intermittent soft contact assessments of $\Delta E/E$ is attributed to error propagation resulting from the relative complexity of terms, the approximations used, and the number the terms encountered in the respective model calculations. Nonetheless, the agreement between the RDF-AFUM and the intermittent soft contact assessments is quite good considering that the calculations are performed on rather disparate equations. More importantly, the agreement between the model predictions and the measurements from independent mechanical tests provides quite strong evidence for the general validity of the present model.

The present model can also be used to quantify the image contrast from variations in the sample absorption coefficient γ_s or from a combination of absorption coefficient and Young modulus variations in the material. Space limitations prohibit the inclusion of such contrast mechanisms here, but the effects can be derived straightforwardly by the reader from the equations derived above. Although the present model is developed for flexural oscillations of the cantilever and out-of-plane vibrations of the sample surface, the model can in principle be extended to include other modes of cantilever oscillation and sample surface response. It is anticipated that such a development would provide

even greater opportunities for obtaining quantitative information on material properties using the various A-AFM modalities.

REFERENCES

a Electronic mail: john.h.cantrell@nasa.gov

b Electronic mail: sac3k@virginia.edu

1. G. Binnig, C. F. Quate, and Ch. Gerber, Phys. Rev. Lett. **56**, 930 (1986).
2. P. Maivald, H. J. Butt, S. A. Gould, C. B. Prater, B. Drake, J.A. Gurley, V. B. Elings, and P. K. Hansma, Nanotechnology **2**, 103 (1991).
3. U. Rabe and W. Arnold, Appl. Phys. Lett. **64**, 1493 (1994).
4. U. Rabe, S. Amelio, M. Kopychinska, S. Hirsekorn, M. Kempf, M. Goken, and W. Arnold, Surf. Interface Anal. **33**, 65 (2002).
5. O. Kolosov and K. Yamanaka, Jpn. J. Appl. Phys. **32**, L1095 (1993).
6. K. Yamanaka, H. Ogiso, and O. Kolosov, Appl. Phys. Lett. **64**, 178 (1994).
7. M. T. Cuberes, H. E. Alexander, G. A. D. Briggs, and O. V. Kolosov, J. Phys. D: Appl. Phys. **33**, 2347 (2000).
8. G. S. Shekhawat and V. P. Dravid, Science **310**, 89 (2005).
9. S. A. Cantrell, J. H. Cantrell, and P. T. Lillehei, J. Appl. Phys., in press.
10. L. Muthuswami and R. E. Geer, Appl. Phys. Lett. **84**, 5082 (2004).
11. D. C. Hurley, K. Shen, N. M. Jennett, and J. A. Turner, J. Appl. Phys. **94**, 2347 (2003).
12. R. E. Geer, O. V. Kolosov, G. A. D. Briggs, and G. S. Shekhawat, J. Appl. Phys., **91**, 9549 (2002).
13. O. V. Kolosov, M. R. Castell, C. D. Marsh, and G. A. D. Briggs, Phys. Rev. Lett. **81**, 1046 (1998).

14. G. G. Yaralioglu, F. L. Degertekin, K. B. Crozier, and C. F. Quate, J. Appl. Phys. **87**, 7491 (2000).

15. H. B. Chan, V. A. Aksyuk, R. N. Kleiman, D. J. Bishop, and F. Capasso, Phys. Rev. Lett. **97**, 211801 (2001).

16. J. H. Cantrell, J. Appl. Phys. **96**, 3775 (2004).

17. U. Rabe, K. Janser, and W. Arnold, Rev. Sci. Instrum. **67**, 3281 (1996).

18. J. H. Cantrell, "Fundamentals and applications of nonlinear ultrasonic nondestructive evaluation," in *Ultrasonic Nondestructive Evaluation: Engineering and Biological Material Characterization*, edited by Tribikram Kundu (CRC Press, New York, 2004), pp.363.

19. R. Truell, C. Elbaum, and B. Chick, *Ultrasonic Methods in Solid State Physics* (Academic, New York, 1969).

20. C. C. Fay, D. M. Stoakley, and A. K. St. Clair, High Performance Polymers **11**, 145 (1999).

FIGURE CAPTIONS

Fig.1. Schematic of cantilever tip-sample surface interaction: Left side shows relative positions of the cantilever tip and sample surface in the presence of an interaction force. Right side shows spring model representing the dynamics of the tip-surface interaction. z_0 is the quiescent tip-surface separation distance, z the oscillating tip-surface separation distance, η_c the displacement (positive down) of the cantilever tip , η_s the displacement of the sample surface (positive up), k_{cn} is the nth mode cantilever spring constant, m_c the effective cantilever spring mass, k_s the sample spring constant, m_s the effective sample spring mass, and $F'(z_0)$ and $F''(z_0)$ are the linear and first-order nonlinear sample stiffness constants, respectively.

Fig.2. Schematic of interaction force as a function of the separation distance between cantilever tip and sample surface.

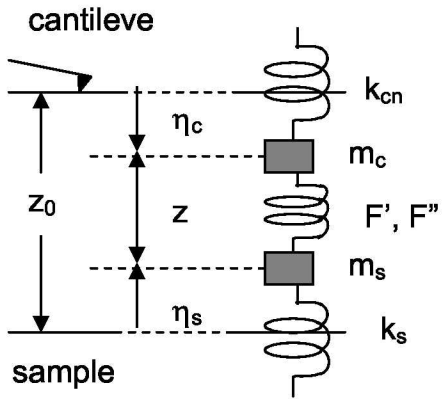

Fig. 1.

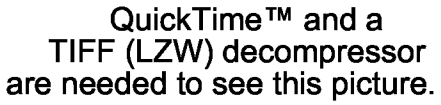
QuickTime™ and a
TIFF (LZW) decompressor
are needed to see this picture.

Fig. 2.